Direct absorption solar collector with magnetic nanofluid: CFD model and parametric analysis

Boris V. Balakin[a,b,*], Oleg V. Zhdaneev[c], Anna Kosinska[a], Kirill V. Kutsenko[b]

[a] *Western Norway University of Applied Sciences, Dpt.Mech.Mar.Eng., Bergen, Norway*
[b] *NRNU Moscow Engineering Physics Institute, Dpt.Therm.Phys., Moscow, Russia*
[c] *Schlumberger, Moscow, Russia*

Abstract

Direct absorption collectors (DAC) with nanofluid are among the most promising yet least studied in solar energy technology. There are numerous micro- and macroscopic factors that determine their efficiency. This complicates *in situ* optimization of DACs using physical prototypes. The present paper describes a multiphase CFD model of the collector, which was validated against two independent experimental datasets. The model was used for a multiparametric numerical analysis, where we altered concentration and size of the nanoparticles, as well as the geometry and inclination of the collector. The optimization resulted in up to 10% improvement in the collector's efficiency. Finally, we considered the process of thermomagnetic convection in the collector using a magnetic nanofluid. This resulted in a 30% increase in the collector performance.

Keywords: direct absorption collector, CFD, multiphase, nanofluid, thermomagnetic convection

1. Introduction

The conventional solar collectors are heat exchangers, equipped with the light-absorbing black surface and a vessel with liquid coolant, that is responsible for evacuation of heat from the surface. The most challenging issue in the design of the collectors is the limitation of radiate thermal loss from the absorbing surface as its temperature increases. A relatively new and alternative type of solar collector, Direct Absorption Collector (DAC) was first documented in the 1970s [1]. In the DAC the coolant, i.e. the heat transfer fluid, flowing through the collector, is used simultaneously for absorption and evacuation of heat. The volumetric absorption of incident solar radiation and limitation of thermal resistance at the contact "absorber-coolant" determines the performance of the DAC.

Nanofluids, which are stable suspensions of Brownian nanoparticles in heat transfer fluids (water, glycol, mineral oil), are currently considered as the most suitable coolants and absorbers for DAC. If a nanofluid is used in a solar collector with a transparent receiver,

*corresponding author, Boris.Balakin@hvl.no

nanoparticles absorb, accumulate and transfer heat at a very high rate to the base fluid. There are numerous types of nanofluids and configurations of the direct absorption solar collectors. At present, it is not entirely clear which of them is the most efficient. In addition, the experimental studies of the nanofluids are very complex considering the limited flexibility for producing a wide range of nanoparticles of varied particle size.

Numerical modelling ought to enlighten main details of photo-thermal phenomena, which are attributive to DAC technology. However, there have been very few, and rather simplistic models, reported so far. Otanicar et al. [1], Ni et al. [2] and Liu et al. [3] described two-dimensional numerical models, capable of predicting temperature profile in the DAC. The models were based on the combination of the Mie scattering theory, used to mimic the absorption of incoming thermal radiation in the nanoparticles and the base fluid, and Fourier's law of heat transfer. The models were validated against in-house experiments. Nevertheless, these models did not account for the convective motion of the nanofluid, which was an assumption, suitable for the collectors, where the optical path of incident radiation was directed opposite the gravitational force as the natural convection was not expected to develop in this case. On the other hand, natural convection is much more intense when the DAC is coupled with a parabolic light concentrator. In this case, the simplified thermal analysis used in the mentioned works is scarcely applicable.

A substantial number of papers report the nanofluid convection in thermal systems without optical absorption of radiation. Most of them are based on the multiphase computational fluid dynamics (CFD), which simulates the dynamics of the base fluid and the nanoparticles. Fard et al. [4] simulated forced convection of aqueous nanofluid with metallic nanoparticles in a long tube of circular cross-section. A more complex and accurate three-phase model for boiling of nanofluids in a vessel of similar geometry was developed by Valizadeh and Shams [5]. Even though the models demonstrated excellent agreement with the experiment (the discrepancies were below 15%), the standard two-fluid model, available under the commercial code CFX, was applied in the studies. The models therefore did not reproduce mechanisms that were specific to the nanoparticles: the Brownian dispersion of the particulate phase and rarefaction effects in the drag model. These effects were accounted by e.g. Rastegar et al. [6], who simulated filtration of 35-600 nm ceria particles from a water-based nanofluid. Nevertheless, the model [6] did not conduct a thermal analysis of the system. An insteresting article has been recently published by Salari et al. [7], who developed a two-phase CFD-model of the nanofluid convection in DAC at different collector sizes, inclinations and volume fractions. The model however considers the nanofluid as a single-phase mixture without account for transport of particulate phase within the base fluid.

As it follows from other previous studies [8, 9], the convective currents may be further enhanced by means of thermomagnetic convection. This phenomenon is attributive to a nanofluid composed of magnetic nanoparticles (ferrofluid). When an external magnetic field is established at the hottest region of the nanofluid, a new convection current is formed due to the difference between the attractive magnetic forces, acting on the cold (stronger force) and the hot (weaker force) nanoparticles. The most recent experimental study by Alsaady et al. [8] considers radiant heating of the ferrofluid in the DAC under the influence of an external magnetic field. The experiments resulted with better photothermal performance

of the collector relative to cases without magnetic field. Nevertheless, due to the limited visual access to the photothermal system, the evolution of the nanofluid in the magnetic field could not be considered and development of thermomagnetic convection was not explicitly confirmed.

To our knowledge, there are no records of CFD models of DACs with thermomagnetic convection in the literature. A very limited number of the multiphase CFD models is developed for this type of convection in general. The model by Aursand et al. [9] has to be mentioned in this context. The authors reproduced numerically heat transfer in a lab-scale flow loop. They made use of third-party experimental data on the magnetization of ferrite nanoparticles and updated the standard multiphase mixture model with a momentum source, which modelled the nanoparticle magnetic force.

In this paper, we describe a multiphase CFD model, which has been used for simulation of the aforementioned features of the process in a greater detail: absorption of the thermal radiation, Brownian forces, rarefaction effects, natural and thermomagnetic convection. Next, the model was validated against experiments and further used for a parametric analysis of the DAC, searching for the optima of the photothermal performance.

2. Methodology

2.1. Model description

The nanofluid is modelled using the Eulerian-Eulerian technique, assuming the both phases (the base fluid and the nanoparticles) constitute two different inter-penetrating fluids, which share the same pressure. The phases are therefore described by two separate systems of Navier-Stokes equations. The continuity reads:

$$\frac{D(\phi_i \rho_i)}{Dt} = 0, \tag{1}$$

where D/Dt is the substantial derivative, ρ_i and ϕ_i are the density and the volume fraction of ith phase; $\sum_i \varphi_i = 1$. Each phase is denoted by $i = p$ for the nanoparticles and $i = c$ for the base fluid.

The momentum equation becomes:

$$\frac{D(\phi_i \rho_i \mathbf{v}_i)}{Dt} = -\phi_i \nabla p + \phi_i \mu_i \nabla^2 \mathbf{v}_i + \phi_i \rho_i \mathbf{g} + \mathbf{M}_{i,j} + \delta_{i,p} \mathbf{M}_B, \tag{2}$$

where $\mathbf{v}$ is the velocity, p is the pressure, μ is the dynamic viscosity, $\delta_{i,j}$ is Kronecker's delta and $\mathbf{g}$ is acceleration due to gravity; $\mathbf{M}_{c,p} = -\mathbf{M}_{p,c}$ is the inter-phase momentum transfer term, and $\mathbf{M}_B$ is the momentum, induced in the nanoparticle phase due to the Brownian motion in the base fluid.

The energy equation is written as in [6]:

$$\frac{D(\phi_i \rho_i e_i)}{Dt} = \nabla(\phi_i k_i \nabla T_i) + q_{i,j} + q_{v,i}, \tag{3}$$

where $e_i = C_{p,i}T_i$ is the phase specific enthalpy, k_i is the thermal conductivity, T_i is the temperature, q_v is the volumetric heat generation due to absorption of radiant heat by phases and $q_{i,j}$ is the inter-phase heat transfer term, which is, assuming convective heat transfer between the nanoparticles and the base fluid, is computed in accordance with the Ranz-Marshall expression [10].

The inter-phase momentum transfer term is given by the superposition of the drag forces from the particles residing in a computational cell: $\mathbf{M}_{c,p} = (6\phi_p/d^3)\mathbf{F}_D C_c^{-1}$, where d is the average diameter of the nanoparticles; $\mathbf{F}_D$ is the drag force, calculated using the standard expression by Schiller-Naumann [10]. The drag force was additionally updated with Cunnigham's correction to account for rarefaction effects, attributive to nanoparticles [10]:

$$C_c = 1 + Kn\left(2.49 + 0.84\exp\left[-1.74/Kn\right]\right), \tag{4}$$

where $Kn = \lambda/d$ is the Knudsen number and λ is the molecular free path in the base fluid. The displacement of the light nano-sized particles is affected by the Brownian motion in the base fluid. The momentum source term, acting on the nanoparticles from the fluid, is given with a probabilistic expression, obtained by Dong et al. [11], who solved the Langevin equation for the motion of a single particle in Brownian liquid:

$$\mathbf{M}_B = \phi_p\rho_p\sqrt{\pi S_0/\Delta t}\left(\xi_1\mathbf{e_x} + \xi_2\mathbf{e_y} + \xi_3\mathbf{e_z}\right), \tag{5}$$

where ξ_1, ξ_2, ξ_3 are zero-mean and unit-variance Gaussian random numbers, generated independently of each other within a solution time step Δt; and $\mathbf{e_x}$, $\mathbf{e_y}$, $\mathbf{e_z}$ are the unit vectors of the Cartesian coordinate system. The spectral intensity of Brownian fluid-particle interactions S_0, is adopted from Rastegar et al. [6]:

$$S_0 \approx 21.9\frac{\mu_c}{\rho_p^2}\cdot\frac{k_B T_c}{d^5 C_c}. \tag{6}$$

Here k_B is the Boltzmann constant.

Assuming the external radiant heat flux is absorbed in the nanofluid according to Beer-Lambert's law [2], the solar radiation is modelled using the volumetric energy source q_v:

$$q_{v,i} = q_0 K_i \exp\left[-\left(K_c + K_p\right)l\right], \tag{7}$$

where l refers to the optical path in the direction, orthogonal to the boundary, exposed to the external radiant heat flux q_0. Following Taylor et al. [12], we note that attenuation of the solar light in the nanofluid occurs primarily due to absorption of the light in the base fluid and at the surface of the nanoparticles, while its scattering was an order of magnitude smaller. The extinction coefficient of the nanoparticles K_p was therefore approximated as: $K_p \approx (\phi_p/d)\,Q_{abs}$, where the absorption efficiency is found according to the Mie scattering theory [13] for each separate wavelength. The wave length-based approach, although most accurate, is nevertheless expensive in terms of numerical computation. We therefore simplify the expression for the extinction coefficient, using an average constant $Q_{abs} \approx 6$, assuming, similarly to Liberman et al. [14] and Ulset et al. [15], perfect absorption of light at the entire surface of a single nanoparticle.

2.2. Experimental benchmarks

The developed model was firstly used to simulate a laboratory scale collector system described in Liu et al. [3]. In their study a cylindrical column of nanofluid (ID 10 cm) of variable height (up to 7.5 cm) was exposed to an emulated solar radiation (SOLAREDGE 700) of $q_0 = 2.3$ sun from the top edge. A schematic description of their experimental system is presented in Fig. 1A. The nanofluid was produced by means of sonication of [HMIM]BF4 ionic fluid (1-Butyl-3-methylimidazolium tetrafluoroborate, $\lambda \approx 0.7$ nm, estimated from Sigma-Aldrich datasheet [16]) and graphene nano-clusters with length $d \approx 500$ nm [17]. The measurement system included eleven K-type thermocouples ($\pm$ 0.01 K), which were located along the centerline of the column with an increment of 10 mm. The nanofluid cylinder was veiled with a layer of thermally insulating low-density foam from the sides; our estimate of the thermal resistance for the insulation is 21.8 K/W. The bottom of the receiver was protected with a much thicker layer of the same foam and therefore can be assumed adiabatic. The molecular properties of the base fluid and their dependence on temperature ($C_{p,c}(T_c)$, $k_c(T_c)$, $\rho_c(T_c)$ and $\mu_c(T_c)$) were taken from the original study [3] and another paper by the same authors [18]. The properties of the graphene were found in Pop et al. [19]. Due to the very low volume fraction of particles, considered in the reference experiment and in our model (up to 0.1%), the possible change of viscosity of the nanofluid was insufficient. The granular viscosity of the particulate phase was therefore set equivalent to the viscosity of the base fluid $\mu_p \approx \mu_c$.

The second experimental dataset was produced in-house and reported in detail elsewhere [15]. The experiments were aimed at studying the process of the photothermal evaporation of a nanofluid with 0.9% of carbon black nanoparticles (51$\pm$17 nm), dispersed in water by means of sonication in an ultrasound bath Branson 3510 (320 W). Considering granulometry of the nanofluid after the experiments using optical microscopy and static light scattering (Fritsch Analysette 22), we noted agglomerated nanoparticles of sizes up to 7 μm with a mean at $\approx$1.5 μm. A cylindrical glass tube (ID 13.5 mm, height 148.0 mm) with the nanofluid (column height 36.4 mm) was illuminated by two halogen lamps (OSRAM Haloline 400 W) of 5.76$\pm$0.40 sun each. The nanofluid temperature was controlled by a T-type thermocouple (Omega, $\pm$0.3K), which was located at 131 mm from the top of the tube. The in-house experimental system and heating configuration are schematically shown in Fig.1C.

2.3. Boundaries and model set-up

The boundary conditions of the model included constant atmospheric pressure at the top of the simulated column and the no-slip walls for both phases on the rest of the cylindrical surface (see Figs.1A–C). The thermal conditions, however, were different at these boundaries. Initially we reproduced the experiment by Liu et al. [3] (Fig.1A), assuming an adiabatic wall at the bottom of the cylinder, and a convective-radiate heat loss q_s at the rest of the surface. The standard expressions, presented in the supplementary materials, were used to calculate thermal losses. Considering orientation of the experimental system in the field of gravity it is possible to assume that thermal conduction was the most dominant heat transfer mechanism during the experiments by Liu et al. [3] because natural convection of

the nanofluid was apparently not developed there. This model configuration is denoted as "conduction" in Fig.1A.

We further suggested that convective mixing would improve the photothermal performance of the system. Therefore, the first model was compared to a numerical model of an equivalent system, where the radiant heat flux q_0 fell to the bottom of the nanofluid column while the rest of the model parameters were kept as in the case from Fig.1A. The configuration of thermal boundary conditions, presented schematically in Fig. 1B was altered in this case: the adiabatic condition was set at the top pressure boundary; the radiate-convective heat flux q_s was specified at the bottom of the vessel, where we assumed the wall was transparent to receive radiant heat. This heating configuration was considered as a reference for a sensitivity analysis, where the concentration and size of the nanoparticles were altered. Next, to mimic possible changes of collector tilt angle, we studied how orientation of the nanofluid column in the field of gravity influences the process. This model is denoted as "conduction" in Fig.1B.

The last heating configuration, shown in Fig.1, reproduced the in-house experiment by Ulset et al. [15]. This supplementary model was constructed to double-verify our simulation approach and did not undergo a parametric analysis. To account for evaporation of water, registered experimentally even at early stages of photothermal heating, following Ni et al. [2], we increased the heat transfer coefficient at the top boundary by a factor $\times 17$. This model is denoted as "in-house" in Fig.1C, where the spatial orientation of lamps is presented in two projections.

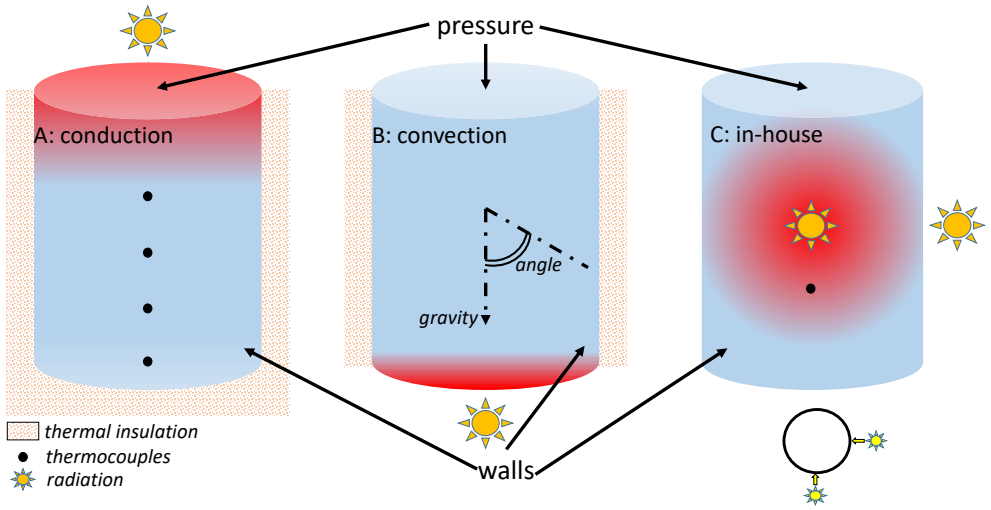

Figure 1: Schematic presentation of heating alternatives and boundary conditions

The initial conditions of the models included zero velocity field in both phases, $T_c = T_d = T_a$, where index a denotes surrounding air. A uniform distribution of the particulate phase over the entire system at the concentration $\phi_{p,0} = 5$ ppm for the "conduction" and

"convection" cases [3] and $\phi_{p,0} = 9000$ ppm for the "in-house" case.

Equations (1-3) were discretized in the commercial CFD package STAR-CCM+ using central differences over a uniform cubical 3-mm grid for the "conduction"-"convection" configurations. The grid size was selected after the grid independence study, considering cells of 1, 2, 3, 4, 5, 6 mm. The grid size was chosen when balancing numerical dispersion and computational costs, especially taking into account that the experimental physical time was more than 400 s. The model of the in-house experiment was discretized with smaller 1-mm cells to reproduce curvature at the bottom of the glass tube. In the "in-house" case we used the molecular properties water (IAPWS-IF97) and carbon, available directly from STAR-CCM+. The temporal discretization was based on the 2^{nd} order Euler implicit technique with $\Delta t = 5$ ms. The equations were solved using the commercial CFD package STAR-CCM+ 12.02.011, running in parallel at 8 cores of 2.5 GHz. The numerical solution was obtained using the SIMPLE technique; the following relaxation coefficients were applied: 0.1 for pressure, 0.3 for velocity, 0.5 for phase volume fraction.

3. Results and discussion

3.1. Conduction vs. convection

The first simulation dataset was produced for the top heating configuration ("conduction" case). The validation plot, presented in Fig. 2A, demonstrates how the axial profile of the excess temperature ($\Delta T = T_c$ - T_a) changes with time in the system.

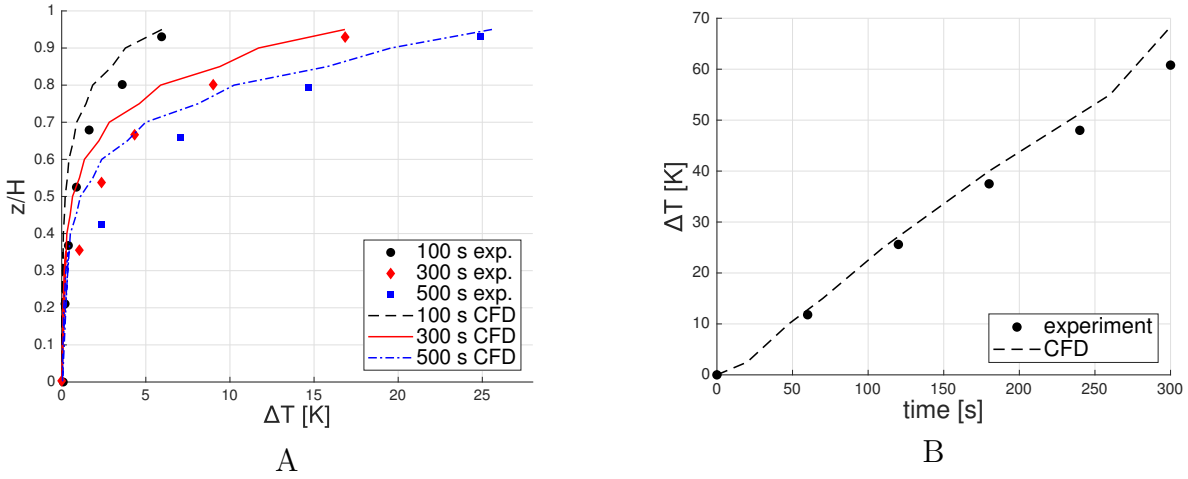

Figure 2: A – temperature profile at 100, 300, 500 s of the process, reported by Liu et al. [3]. B – excess temperature as a function of time during the in-house experiment [15]. The CFD results are compared with the experiment.

This figure depicts the existence of a sharp temperature gradient up to ≈1280 K/m at the top thermal layer of the nanofluid. The gradient continuously grows throughout the entire duration of the process. This temperature profile established because the rate of the radiant heat consumption in the nanofluid exceeded the rate of conductive internal heat

transfer within the collector. A similar temperature profile was obtained by, for instance, Ni et al. [2], Bhalla and Tyagi [20], Liu et al. [21]. The numerical results overestimate the experimental data with an average discrepancy of about 20%. The deviation result from the constant-wavelength simplification taken in the calculation of the extinction coefficient K_i. Additional discrepancies originate from uncertainties, connected to our estimates of thermal resistance of insulating foam and determination of particle size. The results of the second validation against the supplementary experimental dataset are presented in Fig.2B. Here we note almost linear increase of the nanofluid temperature up to the boiling point. The model reproduces the experimental data with the time-average discrepancy below 10%.

Figure 3: Streamlines of fluid velocity at 500 s of the process. Irradiation from the top (conduction) and the bottom (convection) of collector.

Figure 3 shows streamlines of the base fluid after 500 s of process. For the case when the radiation was from the top, two velocity patterns are noticeable: a relatively fast flow of the base fluid in the top boundary layer; and a low-magnitude convective pattern in the rest of the nanofluid column. The top boundary layer is formed primarily due to the downward motion of the hot nanoparticles, which move under the gradient of the Brownian forces (and so the temperature gradient) and settle. The dynamic viscosity of the ionic

fluid, considered in this study, is about two orders larger than the viscosity of water (70-200 mPa·s). The maximum magnitude of the convective patterns is therefore up to 0.2 mm/s, which is significantly lower when compared to the natural convection of air or water. Moving towards the bottom, the nanoparticles release most of their excess heat to the base fluid in the closest vicinity of the top boundary, within the optical depth of the nanofluid. A minor convective flow pattern however rises from the bottom of the column. This vortex originates from the Rayleigh-Taylor instability and does not contribute to establishment of the Rayleigh-Benard convection, which is confirmed with a low value of Rayleigh number Ra=25. When the nanofluid column is radiated from the bottom, the density gradient in the base fluid is responsible for the establishment of the well-recognized convective patters at Ra=$8.1 \cdot 10^5$. The convective flow patterns for the second configuration are shown in Fig. 3. The influence of the particulate phase is not explicitly seen from the flow profile, the size of which is an order-of-magnitude higher than in the conductive case. In the "in-house" case we detected an asymmetric Rayleigh-Bernard convective pattern at Ra=$2.0 \cdot 10^6$, originating from the irradiated walls. Due to the higher concentration of nanoparticles, there were also much stronger Rayleigh-Taylor vortices detected in the model of the in-house system. This information is provided in the supplementary materials.

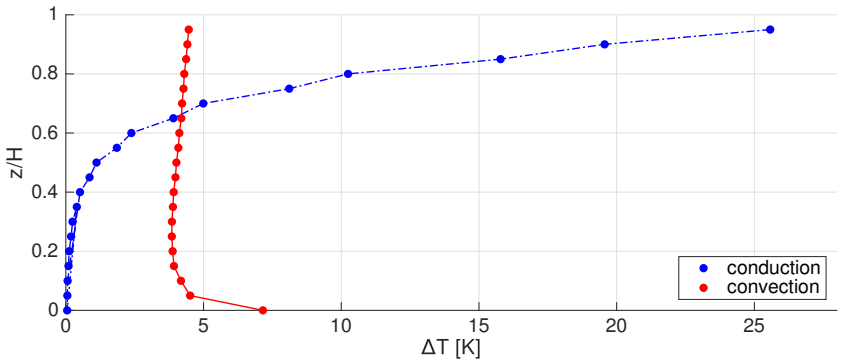

Figure 4: Temperature profile at 500 s of the process. Irradiation from the top (conduction) and the bottom (convection) of collector.

Considering temperature distribution along the centreline of the collector in Fig. 4, we notice more uniform heating of the nanofluid than in the conductive case. A slight variation of the excess temperature in the interval 3.8-4.3 K is detected over almost the entire volume of the nanofluid except for the thin layer at the bottom boundary, exposed to radiation. Here the excess temperature increased to 7.2 K. A qualitatively similar temperature profile for a convective photo-thermal heating of nanofluid with gold nanoparticles was reported by Jin et al. [22].

Fig. 5 compares profiles of the volume fraction (relative to initial value ϕ_0) for the conductive and convective heating configurations. In the first case, the volume fraction is maximum at the bottom of the collector due to sedimentation of the nanoparticles, while the dilute region is observed at the top boundary. As expected, a relatively uniform concentration

profile is observed in the second case because the dispersed phase becomes homogeneously distributed over the entire system with the convective currents. Better absorption of radiant heat happens in this system.

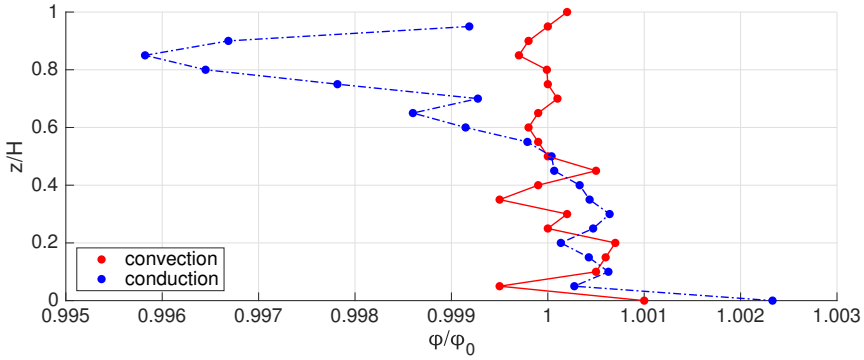

Figure 5: Volume fraction profile at 500 s of the process. Irradiation from the top (conduction) and the bottom (convection) of collector.

3.2. Absorption efficiency

The photothermal performance of the solar collector is characterized by the absorption efficiency, which is the ratio of the harvested radiant heat to the total incident solar energy. In contrast to the standard definition of the collector efficiency (ASHRAE 93-77 [23]), determined by the thermal energy evacuating from the collector to an external heating network, here we consider the dynamics of heating for an isolated solar batch:

$$\eta_a = \frac{m_{NF}\overline{C}_{NF}\left(d\overline{T}/dt\right)}{q_0 A_s}, \tag{8}$$

where m_{NF} is the total mass of the nanofluid in the collector. Furthermore, $\overline{C}_{NF} = \overline{(\phi_c C_{p,c} + \phi_p C_{p,p})}$ and $\overline{T}$ are the volume-average specific heat and the temperature of the nanofluid, respectively, and A_s is the exposed surface area.

The absorption efficiency of the collector is shown in Fig. 6 for different heating configurations. Analyzing the histogram, we conclude that by increasing the collector height from 1.0 to 7.5 cm, the efficiency increases by 28% in the case of the convective heating because the convective currents gain better intensity for a higher nanofluid column with the sufficient density gradient. It is important to note that our results are in qualitative agreement with the experiments of Liu et al. [3] who detected a reduction in the photothermal performance for lower collectors.

Comparing the conductive case with the convective heating configuration for the same collector height of 7.5 cm, we note 6% enhancement for the latter case (81% vs 75%). The volume-average magnitude of the base fluid vorticity is 19 times higher in the convective case. It is important to note that, although this result is qualitatively predictable, here we

provide a quantitative estimate of the efficiency gain for the convective heating configuration. Another interesting observation comes from the comparison between DAC collector with nanofluid and a flat plate collector with opaque walls, filled with the base fluid without nanoparticles. The collectors are of equivalent size. The photothermal performance of the flat plate collector becomes 11% and 5% lower than for DAC in the conductive and the convective configurations, respectively (Fig. 6). The volumetric absorption of the radiant heat is more efficient than in the flat plate case, since the total area of the solids, harvesting the sunlight within the penetration depth, is equivalent to the absorption area of the flat-plate-collector, while the absorption in the base fluid comes in addition. The contrast is sharper for the conductive case due to the less intensive evacuation of heat from the hot boundary and the consequently larger radiate losses. These values correspond well with the experimental observations recorded by Otanicar et al. [1] and Karami et al. [24] who noticed up to 5% efficiency enhancement for the DAC in comparison with the flat plate configuration.

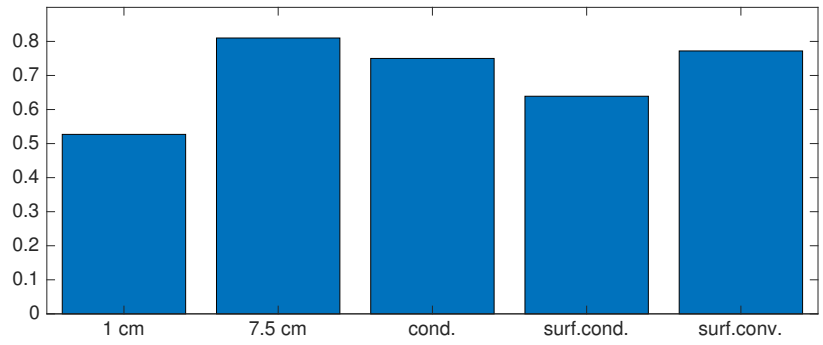

Figure 6: Thermal efficiency for different configurations: DAC height (1 cm, 7.5 cm) with irradiation from the bottom; irradiation from the top for 7.5 cm DAC (cond.); convection (surf.conv.) and conduction (surf.cond.) in an opaque flat plate collector without nanoparticles.

The geometry of the system and the type of the base fluid are determined by a number of macroscopic factors such as the available collector area, capital costs, freezing and the flash point etc. The concentration and the size of the nanoparticles are the microscopic parameters that enable a relatively simple fine-tuning of the collector efficiency when the macroscopic parameters are fixed. Figs. 7-8 demonstrate the dependence of the absorption efficiency for 1-cm DAC on these two variables. The simulation results reveal the existence of a maximum efficiency of 64% that corresponds to $\phi_p = 10$ ppm and $d_p = 100$ nm. Below this concentration the efficiency decreases as the number of particles in the collector is insufficient for the effective absorption of thermal radiation. The penetration depth reduces dramatically when the concentration is above the detected optimum. The collector appearance comes closer to the flat-plate configuration in this case as the particles attenuate most of the radiation in the closest vicinity of the outer boundary. The existence of the optimum of the photothermal performance was documented in a number of experimental works. Liu et

al. [21] obtained an optimum of absorption efficiency of 40 % at 1.25 ppm in the reduced graphene oxide nanofluid with the particle size up 1000 nm. Wang et al. [25], who considered photothermal heating of an aqueous nanofluid with 13-nm gold nanoparticles, reported the optimum of 25% at 23.5 ppm. Finally, in our previous work [15] we registered maximum η_a = 66% at 3% wt. in the aqueous nanofluid with the agglomerated up to 7 μm carbon black nanoparticles.

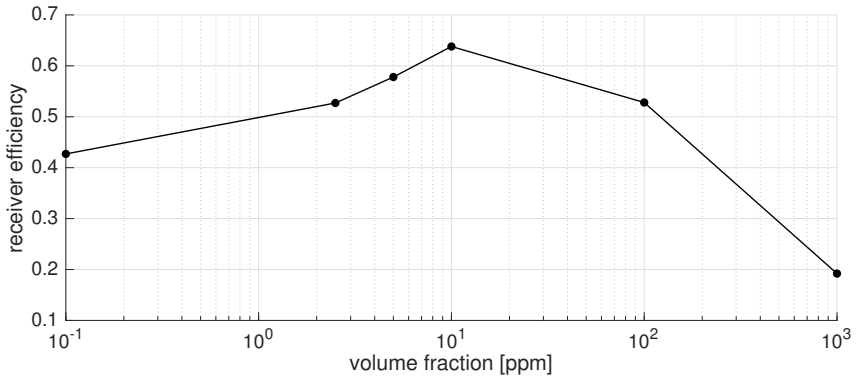

Figure 7: Thermal efficiency of 1-cm DAC as a function of nanoparticle volume fraction.

The collector exhibits similar behaviour when the particle size is altered (Fig. 8): when the particle size is reduced at the fixed concentration, their number density grows, increasing the attenuation; the largest particle sizes reside in the most diluted nanofluid, where the absorption goes mainly in the base fluid. There is a limited number of works on the influence of the nanoparticle size on the photothermal performance of the collector due to the complexity of the controlled size manipulation. The study by Guo et al. [26] has to be noted in this context since they report the photothermal optimum of 5.2% for 37.8-nm gold nanoparticles.

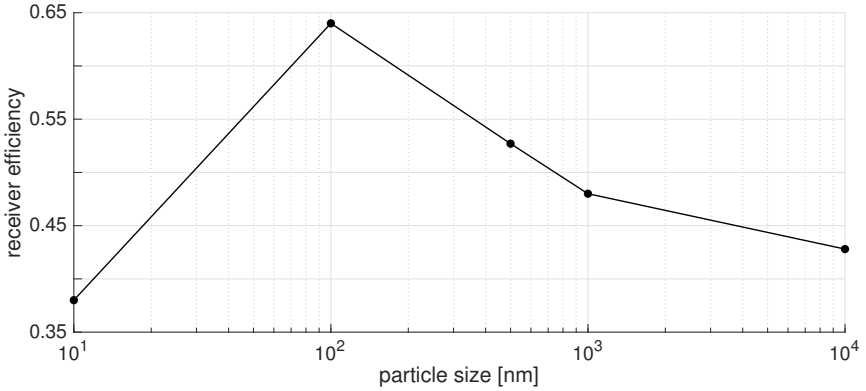

Figure 8: Thermal efficiency of 1-cm DAC as a function of nanoparticle size.

Following the discussions presented above, we concluded that the collector efficiency is indubitably dependent on the intensity of convective currents, which, in turn, are determined by the height of convective cells that establish along DAC. This parameter is directly related to the mutual orientation between the gravity field and the direction of thermal radiation, which is not always constant *in-situ* due to variation of solar azimuth.

At the end of this section, we examine how sensible the absorption efficiency becomes relative to orientation of the collector in the field of gravity. The inclination of the collector was simulated altering the magnitude and direction of $\mathbf{g}$ in Eq. (2). The simulations were performed in the convective configuration, when the collector was irradiated from the bottom. The results are presented in Fig. 9, where the collector efficiency is plotted against the angle between $\mathbf{g}$ and the centreline of the collector. The angle is schematically shown in Fig. 1B. Reading the plot from Fig. 9, we note the efficiency drops from 53% (convective case) down to 28% (gravity in horizontal direction). This happens due to reduction in size of convective patterns, which was also demonstrated by Salari et al. [7]. As the angle is further increased, the system drifts to the case, similar to conductive so that the efficiency is restored to a lower level due to the thermal losses.

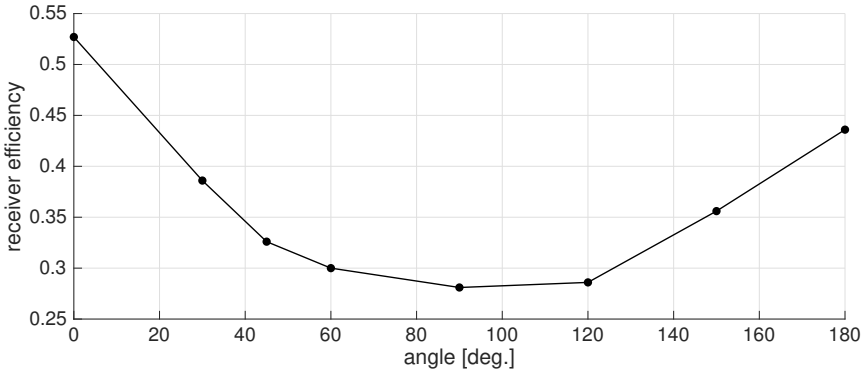

Figure 9: Thermal efficiency as a function of 1-cm DAC orientation.

3.3. Thermomagnetic convection

As demonstrated in the previous sections, the photothermal performance of the solar collector is strongly dependent on the degree of flow agitation in the collector. We further evaluate a potential strengthening of the convective current, studying a ferrofluid under the influence of an external magnetic field in the same geometry of the collector. The model will reproduce the process of thermomagnetic convection (TMC). Modelling the TMC, we update the right-hand-side of Eq. (2) with a new momentum source term, originating from the Kelvin force, acting on the particles [9, 27]:

$$\mathbf{M_m} = -\mu_0 M \frac{dH}{dl} \cdot \frac{\mathbf{l}}{l}, \tag{9}$$

where μ_0 is the magnetic permeability of vacuum and H is the magnetic field. The magnetization of the nanoparticles M is given in Aursand et al. [9] as:

$$M = M_s \mathcal{L}\left(V_p M_s \mu_0 H / k_b T_c\right), \mathcal{L}\left(x\right) = \coth x - 1/x. \tag{10}$$

In Eq. (10), V_p is the volume of the particle. The saturation magnetization M_s depends on the type of the nanoparticles. In this part of the work, similarly to Aursand et al. [9**?**] we consider MnZn ferrite nanoparticles with known magnetic properties:

$$M_s = M^* \left(1 - \left(T_c - T^*\right) / \left(T^{**} - T^*\right)\right), \tag{11}$$

where $M^* = 265$ kA/m, $T^* = 300.1$ K are the reference values and $T^{**} = 576$ K is the Curie temperature. Eq. (11) is valid when $T_c < T^{**}$; when the temperature of the fluid exceeds T^{**}, the magnetization turns to zero.

The numerical simulations of the solar collector with TMC were carried out for the geometry and the combination of boundary condition shown in Fig. 1B, i.e. representing the case when the thermomagnetic convection supplements the natural convection. Following Aursand et al. [9], the properties of the nanoparticles were set as: $d_p = 8$ nm, $\rho_p = 5323$ kg/m^3, $\lambda_p = 5$ W/mK, $C_{p,p} = 704.5$ J/kgK. As in many solar collector applications, the distilled water was used as the base fluid. The initial concentration of the nanoparticles was $\phi_{p,0} = 0.5$ ppm. The magnetic field parameters were of a similar order as considered in [9], namely $H = 90$ kA/m. The magnetic field was assumed to decay linearly towards the top boundary, modelling the case when a magnet is located at the bottom of the system. This is schematically shown in Figure 10 (right). The magnetic field, selected for this study was below 115 mT, which is produced by a majority of low-power electromagnets (e.g. [8], [9]) and permanent magnets [28]. To highlight the influence of the magnetic convection, a comparative simulation was carried out for the case when the natural convection was solely established in the water-ferrite nanofluid.

The simulation results are depicted in Fig. 10, where the excess temperature profile in the collector is compared with the profile resulting from the natural convection. The average excess temperature is 15% lower when TMC is present in the system. There is a temperature gradient formed in the bottom part of TMC-collector. Examining the streamlines of the base fluid for these cases in Fig. 11 we note that centres of the convective cells migrate in the direction of the magnetic attraction. The magnitude of the convective currents and the vorticity increases ≈ 4.0 and 3.4 times in the magnetic system due to the enhanced agitation of the particulate phase.

The volume fraction profiles for both systems are shown in Fig. 12. The distribution of the nanoparticles in the magnetic system is less homogeneous: there is a packed boundary layer of nanoparticles at the bottom boundary. The volume fraction there is 60% over the mean due to the magnetic attraction of the nanoparticles in this region. The concentration recovers to the initial value at about 20% of the collector height. This corresponds to the point, where the temperature profile gets to the minimum as shown in Fig. 10.

The absorption efficiency of the TMC system is presented in Fig. 13 for different values of the magnetic field gradient. This sensitivity analysis reveals that η_a grows with the

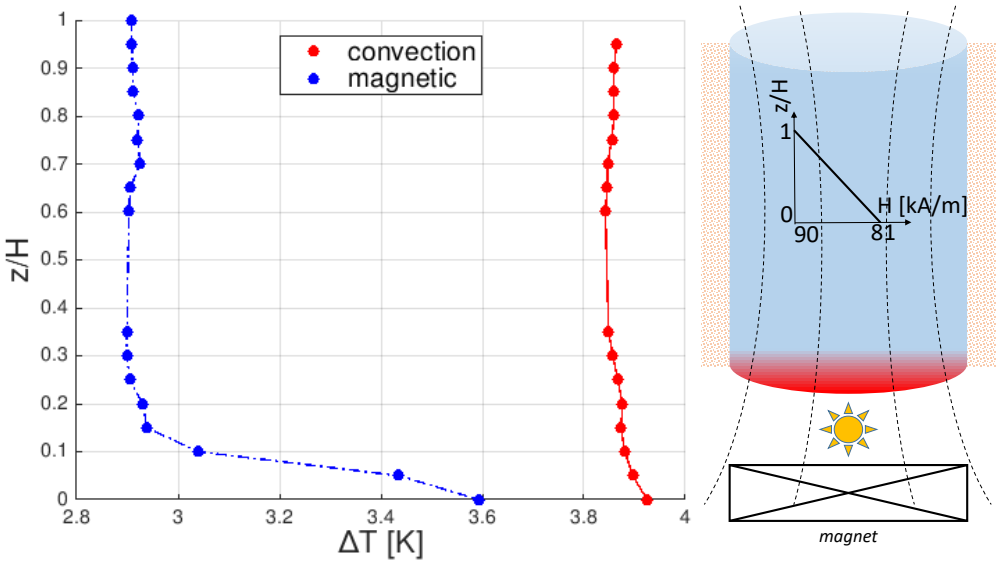

Figure 10: Left: temperature profile at 700 s of the process. Natural convection and thermomagnetic convection. Right: schematic description of DAC with thermomagnetic convection.

gradient, increasing up to 30% (Ra=$96.8{\cdot}10^6$) relative to the case with the natural convection (Ra=$3.2{\cdot}10^6$). This corresponds well to the recent experimental results by Alsaady et al. [8] who observed a 1.35-fold increase in collector efficiency for 20-nm Fe_3O_4 aqueous ferrofluid with TMC.

A significant reduction of collector efficiency takes place, however, at $\nabla H = 252$ kA/m^2. This is caused by a strong attraction of the nanoparticles to the bottom boundary, which results in a formation of a packed stationary layer of the nanoparticles. This consumes most of the incident radiation and hinders natural convection. The optimum value of the magnetic field gradient is approximately the condition, at which the superposition of $\mathbf{M_m}$, $\mathbf{M_{i,j}}$ and $\phi_p \rho_p \mathbf{g}$ are balanced in Eq. (2).

4. Conclusions

This contribution presents a Eulerian-Eulerian two-phase CFD-model of the direct absorption solar collector with nanofluid. The model is capable of reproducing motion and heat transfer in each separate phase: the base fluid (continuous) and the nanoparticles (dispersed). The particulate phase follows the base fluid via the inter-phase momentum transfer and Brownian terms. The model was validated with the third-party experimental data, demonstrating satisfactory agreement.

The sensitivity of the studied virtual direct absorption collector was considered by altering the parameters that determine the photothermal performance of the system. The parametric analysis reveals crucial importance of the convective mass transfer for the system of this type: the convective absorption results in 6% efficiency gain relative to the conductive case, while the volumetric absorption system is up to 11% more efficient than a

Figure 11: Streamlines of fluid velocity at 700 s of the process. Natural convection (top) and thermomagnetic convection (bottom).

conventional flat plate collector. The efficiency also depends on orientation of the collector in the field of gravity, approaching the maximum when the direction of the incident radiation is opposite to the direction of the gravitational force. The simulations demonstrate the existence of optimum particle size and concentration, which correspond to the best efficiency of the collector. Therefore, the model enables tailoring the nanofluid for a very controlled absorption of heat. In addition, we simulated thermomagnetic convection established in the same solar collector, filled with ferrofluid. Again, the model demonstrates the existence of the optimum gradient of magnetic field, and generally the magnetic Rayleigh number. In this condition, the collector efficiency amounts to 30% relative to the non-convective case. Technically this means that the thermomagnetic convection, established artificially in the DAC, may compensate for reduced natural convection when the solar angle is lowered and so to sustain best collector efficiency longer. The simulation results were in qualitative correspondence with experiments carried out for similar thermal systems.

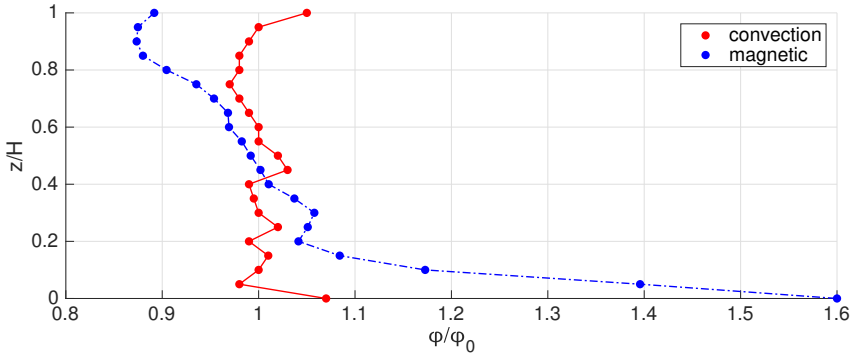

Figure 12: Volume fraction profile at 700 s of the process. Natural convection and thermomagnetic convection.

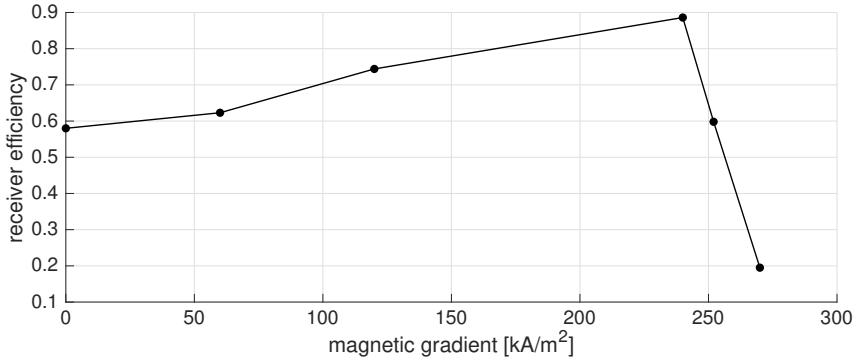

Figure 13: Thermal efficiency as a function of magnetic field gradient.

Acknowledgements

This study was supported by the Russian Science Foundation (project 17-79-10481). We thank Prof. Dr Xiaoming Fang from South China University of Technology for providing information on particle sizes.

References

[1] T. Otanicar, P. Phelan, R. S. Prasher, G. Rosengarten, R. A. Taylor, Nanofluid-based direct absorption solar collector, Journal of Renewable and Sustainable Energy 2 (2010) 033102.

[2] G. Ni, N. Miljkovic, H. Ghasemi, X. Huang, S. V. Boriskina, C.-T. Lin, J. Wang, Y. Xu, M. M. Rahman, T. J. Zhang, G. Chen, Volumetric solar heating of nanofluids for direct vapor generation, Nano Energy 17 (2015) 290–301.

[3] J. Liu, Z. Ye, L. Zhang, X. Fang, Z. Zhang, A combined numerical and experimental study on graphene/ionic liquid nanofluid based direct absorption solar collector, Solar Energy Materials and Solar Cells 136 (2015) 177 – 186.

[4] M. H. Fard, M. N. Esfahany, M. Talaie, Numerical study of convective heat transfer of nanofluids in a circular tube two-phase model versus single-phase model, International Communications in Heat and Mass Transfer 37 (2010) 91 – 97.
[5] Z. Valizadeh, M. Shams, Numerical investigation of water-based nanofluid subcooled flow boiling by three-phase Euler–Euler, Euler–Lagrange approach, Heat and Mass Transfer 52 (2016) 1501–1514.
[6] V. Rastegar, G. Ahmadi, S. Babu, Filtration of aqueous colloidal ceria slurries using fibrous filters. An experimental and simulation study, Separation and Purification Technology 176 (2017) 231–242.
[7] M. Salari, E. H. Malekshah, M. H. Malekshah, M. Alavi, R. Hajihashemi, 3D numerical analysis of natural convection and entropy generation within tilted rectangular enclosures filled with stratified fluids of MWCNTs/water nanofluid and air, Journal of the Taiwan Institute of Chemical Engineers 80 (2017) 624 – 638.
[8] M. Alsaady, R. Fu, Y. Yan, Z. Liu, S. Wu, R. Boukhanouf, An experimental investigation on the effect of ferrofluids on the efficiency of novel parabolic trough solar collector under laminar flow conditions, Heat Transfer Engineering 0 (0) (2018) 1–9.
[9] E. Aursand, M. A. Gjennestad, K. Y. Lervåg, H. Lund, A multi-phase ferrofluid flow model with equation of state for thermomagnetic pumping and heat transfer, Journal of Magnetism and Magnetic Materials 402 (2016) 8 – 19.
[10] C. Crowe, J. Schwarzkopf, M. Sommerfeld, Y. Tsuji, Multiphase flows with droplets and particles. Second Edition, CRC Press, 2012.
[11] S. Dong, L. Zheng, X. Zhang, S. Wu, B. Shen, A new model for Brownian force and the application to simulating nanofluid flow, Microfluidics and Nanofluidics 16 (2014) 131–139.
[12] R. Taylor, P. Phelan, T. Otanicar, R. Adrian, R. S. Prasher, Nanofluid optical property characterization: Towards efficient direct absorption solar collectors, Nanoscale Research Letters 6 (2011) 1931–7573.
[13] C. Bohren, D. Huffman, Absorption and scattering of light by small particles, New York: Wiley, 1998.
[14] M. Liberman, N. Kleeorin, I. Rogachevskii, N. E. L. Haugen, Mechanism of unconfined dust explosions: Turbulent clustering radiation-induced ignition, Physical Review E 95 (2017) 051101.
[15] E. T. Ulset, P. Kosinski, Y. Zabednova, O. V. Zhdaneev, P. G. Struchalin, B. V. Balakin, Photothermal boiling in aqueous nanofluids, Nano Energy 50 (2018) 339 – 346.
[16] Sigma-Aldrich [HMIM]BF_4 datasheet, `https://www.sigmaaldrich.com`.
[17] X. Fang, M. Perez, personal communication (email), additional information on Liu et al. (2017).
[18] F. Wang, L. Han, Z. Zhang, X. Fang, J. Shi, W. Ma, Surfactant-free ionic liquid-based nanofluids with remarkable thermal conductivity enhancement at very low loading of graphene, Nanoscale Research Letters 7 (2012) 314.
[19] E. Pop, V. Varshney, A. K. Roy, Thermal properties of graphene: Fundamentals and applications, MRS Bulletin 37 (2012) 12731281.
[20] V. Bhalla, H. Tyagi, Solar energy harvesting by cobalt oxide nanoparticles, a nanofluid absorption based system, Sustainable Energy Technologies and Assessments 24 (2017) 45 – 54.
[21] X. Liu, X. Wang, J. Huang, G. Cheng, Y. He, Volumetric solar steam generation enhanced by reduced graphene oxide nanofluid, Applied Energy 220 (2018) 302 – 312.
[22] H. Jin, G. Lin, L. Bai, A. Zeiny, D. Wen, Steam generation in a nanoparticle-based solar receiver, Nano Energy 28 (2016) 397–406.
[23] ASHRAE 93-77, Methods of Testing to Determine the Thermal Performance of Solar Collectors, Springer Berlin Heidelberg, 1978.
[24] M. Karami, M. Akhavan-Bahabadi, S.Delfani, M.Raisee, Experimental investigation of CuO nanofluid-based direct absorption solar collector for residential applications, Renewable and Sustainable Energy Reviews 52 (2015) 793–801.
[25] X. Wang, Y. He, X. Liu, L. Shi, J. Zhu, Investigation of photothermal heating enabled by plasmonic nanofluids for direct solar steam generation, Solar Energy 157 (2017) 35–46.
[26] A. Guo, Y. Fu, G. Wang, X. Wang, Diameter effect of gold nanoparticles on photothermal conversion for solar steam generation, RCS Advances 7 (2017) 4815–4824.
[27] A. Lange, Kelvin force in a layer of magnetic fluid, Journal of Magnetism and Magnetic Materials 241

(2002) 327 – 329.
[28] B. V. Balakin, I. Noty, A. C. Hoffmann, P. Kosinski, The formation of deposit in a magnetic fluid: Numerical and experimental study, Powder Technology 228 (2012) 108 – 114.